Tuning the physisorption of molecular hydrogen: binding to aromatic, hetero-aromatic and metal-organic framework materials*

FABRIZIA NEGRI[A,B,†] AND NADIA SAENDIG[A]

[A]*Dipartimento di Chimica 'G. Ciamician', Universita' di Bologna, Via F. Selmi, 2, 40126 Bologna, Italy*

[B]*INSTM, UdR Bologna, Italy*

Abstract

We present a study on the binding properties of molecular hydrogen to several polar aromatic molecules and to a model for the metal-oxide corner of the metal organic framework materials recently investigated as promising supports for hydrogen storage. Density functional theory employing the Perdew Wang exchange-correlation functional and second order Møller-Plesset calculations are used to determine the equilibrium structures of complexes with molecular hydrogen and their stability. It is found that for most hetero-aromatics the edge sites for molecular hydrogen physisorption have stabilities comparable to the top sites. The DFT predicted binding energies compare favorably with those estimated at MP2 level, and get closer to the MP2 results for increased electrostatic contributions (induced by the polar aromatics) to the intermolecular interaction. Vibrational frequencies are also computed at the DFT level and infrared activities of the H_2 stretching frequency are compared for the various complexes. Pyrrole, pyridine and n-oxide pyridine are predicted to form the more stable complexes among one-ring aromatics. The computed binding energies to metal-organic framework materials are in good agreement with experimental observations. It is suggested that replacement of the organic linker in MOF materials with some of the more efficient aromatics investigated here might contribute to enhance the H_2 storage properties of mixed inorganic-organic materials.

Keywords: *density functional theory, second order Møller-Plesset, metal-organic framework materials, hydrogen storage, carbon based materials*

* In memory of Fernando Bernardi

† Corresponding author

Introduction

The increasing worldwide demand for energy has stimulated the search for alternate sources, among which is the hydrogen technology. One major issue concerns the optimization of the materials for the storage of hydrogen required for mobile applications. Several materials have been considered: carbonaceous materials have been the subject of a recent intense activity in search for alternatives to the use of metal hydrides, cryotechniques, or high pressure tanks [1]. High-surface-area carbon based materials are attractive owing to their light weight, stability and low cost. Unfortunately, their interaction with hydrogen is weak (of the order of 1.2 kcal/mol [2-4]), and this poses serious limits to their storage capacity [5].

Numerous computational studies concerning the interaction of hydrogen molecules with carbon based conjugated systems have recently been published. The interaction energies and the corresponding geometries have been calculated at various levels of theory ranging from density functional theory (DFT) [6,7] to second order Møller-Plesset perturbation theory (MP2)[7-12] and coupled-cluster theory including single, double and perturbative estimate of triple excitations (CCSD(T)) [8].

More recently, mixed inorganic-organic compounds, the metal organic framework (MOF) materials, have attracted considerable interest for their promising storage capacities [13-15]. The hydrogen adsorption sites in MOF materials have been investigated by inelastic neutron scattering [13,16] and by neutron diffraction studies [17,18]. These studies have shown that the two main sites for H_2 adsorption are located close to the metal-oxide corners of the material. Furthermore, an estimate of the binding energy of ca. 0.84 kcal/mol for the main H_2 absorption site in MOF materials has been recently obtained from temperature dependent infrared studies on the activity of the adsorbed H_2 stretching frequency [19]. Several computational studies on the H_2 binding properties of MOF materials have appeared. Some of these concerned the organic linkers in the MOF materials [10-12] and few others have concerned the interaction of H_2 molecules with the metal-oxide corners [9,19]. The general model chosen for the calculations consists in a $OZn_4(CO_2H)_6$ cluster formed by an oxygen-centered Zn_4O tetrahedron surrounded by six formiate groups. Recent studies carried out at MP2 level and with different basis sets have predicted binding energies ranging from 0.54 [19] to 1.64 kcal/mol [9] for H_2 bound at the more stable metal-oxide corner site.

The intrinsically weak surface-adsorbate physical interaction in carbon based materials suggests that one way to increase the affinity for molecular hydrogen is chemical substitution of carbon atoms with hetero-atoms or groups able to perturb the weak carbon-hydrogen interaction by increasing the electrostatic contribution. Aromatic molecules with larger

affinity for molecular hydrogen may form the basis for the synthesis of new generation carbon based materials optimized for hydrogen storage. At the same time these molecules may serve as better performing organic linkers in MOF materials. Prompted by these ideas, we have considered in this work a series of aromatic molecules of increasing size and characterized by the presence of hetero atoms or polar groups and we have explored their complexes with molecular hydrogen with DFT calculations. The same level of theory has been employed to investigate the stability of H_2 sites at the metal-oxide corner of MOF materials. The results of DFT calculations have been selectively supplemented by MP2 geometry optimization of the complexes and calculation of binding energies.

Methods

The model systems studied quantum-chemically are of the type aromatic + H_2, where aromatic indicates a specific aromatic molecule (benzene, BN-benzene, borazine, pyridine, n-oxide pyridine, furan, pyrrole, tiophene, bipyridine, tripyridine, n-phenyl-aniline, pyrene-dione), or MOF + H_2 were we restricted the attention to the interaction of molecular hydrogen to the metal-oxide corner of the MOF material. DFT was used to identify the atomic structures of the complexes and their corresponding binding energies. The well tested generalized gradient functional of Perdew and Wang [20] was employed. Although the dispersion interaction is not properly included in present-day exchange-correlation functionals, it has been suggested [21] that among the available functionals, the Perdew and Wang exchange-correlation functional [20] may be a viable alternative to ab initio methods, owing to its good performance in the prediction of weak complexes [6,21]. Here we have chosen the DFT method since some of the complexes investigated are quite large and also because the polar aromatic molecules investigated should induce more considerable electrostatic contributions to the intermolecular interaction with H_2. With a larger electrostatic contribution the DFT predictions are expected to become more reliable than for pure dispersion interactions. Nevertheless, to validate the quality of DFT predictions, we have computed, for selected complexes, MP2 binding energies at fully optimized MP2 structures. The PW91 functional has been shown to have a small basis set dependence, in contrast to MP2 calculations. For this reason we have adopted the 6-311++G** basis set for all the DFT calculations and the correlation consistent (Dunning) basis set augmented with diffuse functions (aug-cc-pVTZ basis set) [22] for MP2 calculations. Furthermore, the nature of the aromatic-H_2 complexes has been verified by computing vibrational frequencies and the

Natural Bond Orbital (NBO) analysis [23] was carried out on all the optimized structures to obtain natural atomic charges. The computed molecular hydrogen binding energies (BE) have been corrected for the basis set superposition error (BSSE) using the counterpoise correction scheme proposed by Boys and Bernardi [24]. All the calculations were carried out with the Gaussian 03 [25] suite of programs.

FIGURE 1 HERE

Results and discussion

One ring aromatics

Six-atom-rings. Before discussing the complexes of H_2 with one-ring hetero-aromatics or substituted benzenes, we consider benzene itself and its ions. The interaction of benzene with H_2 has been computed in several studies [6-9,11], using DFT, MP2 and CCSD(T) levels of theory. Employing the PW91 functional, we determined only one minimum for the complex shown in Figure 1a, namely with the hydrogen molecule pointing perpendicularly to the plane of the benzene ring. Other orientations of the H_2 molecule above the benzene ring, that is, other top sites, do not correspond to minima. The predicted binding is 0.74 kcal/mol, in agreement with previous calculations at the same level of theory (PW91/6-311++G**)[6]. The binding is underestimated compared to the MP2/aug-cc-pVTZ result of 1.11 kcal/mol (see Table 1), the latter being in agreement with previous calculations at the same level of theory [6,7] and also close to the experimental value of 1.2 kcal/mol of H_2 on graphite [4]. The PW91/6-311++G** result can also be compared with the binding of 0.97 kcal/mol computed [10] at the more sophisticated CCSD(T) level of theory, using the QZVPP basis set [26]. In agreement with the computed larger binding, inspection of the main structural characteristics, shows that the C--H_2 distance is considerably reduced at the higher levels of theory.

Beside neutral benzene, we explored the binding properties of benzene cation and anion. The equilibrium structure of the complex between anionic benzene and H_2 (see Figure 1b) is similar to that of neutral benzene, but the complex is less stable (PW91/6-311++G** BE is 0.51 kcal/mol) as inferred also by the looser structure (the closer of the two hydrogens of H_2 is at 3.286 Å from each carbon atom compared to 3.254 Å in neutral benzene). The complex of benzene cation with H_2 is shown at the bottom of Figure 1. In the minimum energy structure the hydrogen is parallel to the plane of the benzene ring, and it is located above the

ring and over one C-H bond. The computed PW91/6-311++G** BE is 1.05 kcal/mol (see Table 1 and Figure 1). The increased BE of benzene cation, compared to neutral benzene is interesting, although in practical applications the use of charged species would not be desirable to improve the hydrogen storage efficiency in carbon based materials.

FIGURE 2 HERE

As a first example of substituted benzene we have considered two boron-nitride substituted benzenes: in the first case (Figure 2a) two adjacent carbon atoms were substituted with one BN couple. As a second example (Figure 2b) we considered borazine, namely a benzene molecule in which all three couples of carbon atoms have been replaced by BN couples in such a way that boron and nitrogen atoms are alternate. BN materials have been considered as alternatives for hydrogen storage and have shown encouraging properties [27]. The interaction of H_2 with BN-benzene was recently investigated theoretically [11]. The equilibrium structure found by us with PW91/6-311++G** calculations (see Figure 2) is similar to that of unsubstituted benzene, namely with the H_2 molecule on the top of the molecular plane, and oriented almost perpendicularly to it. Its computed BE is also very close to that of benzene, namely 0.73 kcal/mol. Although the calculated interaction for BN-benzene suggests H_2 affinity properties similar to those of benzene, this conclusion may be misleading if one considers this aromatic molecule as the organic linker in MOF materials. Indeed, it has been shown recently that the top site of a dicarboxilated BN-benzene binds much more efficiently molecular hydrogen [11].

The computed BE of the H_2 complex with borazine is considerably lower than that of benzene, namely 0.52 kcal/mol at PW91/6-311++G** (see Table 1). In this case we validated this result by performing MP2/aug-cc-pVTZ calculations and found only a slight increase up to 0.60 kcal/ mol. Notice that in this case the DFT result accounts for 87% of the MP2 computed BE. This moderate BE change is associated, however, to remarkable shortening of the distance between H_2 and the boron or nitrogen atoms of borazine. The reduced interaction, compared to benzene, suggests a worse performance of BN materials (compared to carbon based materials) for H_2 storage, in agreement with recent calculations on the physisorption of H_2 on BN nanotubes [28] and nanocages [29].

FIGURE 3 HERE

FIGURE 4 HERE

Two additional six-atom-ring hetero-aromatics have been considered: pyridine and n-oxide pyridine, whose optimized complexes are depicted in Figures 3 and 4, respectively. In

each case we found two sites for the physisorbed H_2 molecule. In the case of pyridine, we found a remarkably stable edge site (BE of 1.16 kcal/mol at the DFT level, see Figure 3a and Table 1) beside the usual top site whose binding seems reduced compared to benzene (BE of 0.54 at the DFT level, see Figure 3b and Table 1). In the former complex, the H_2 molecule is located on the molecular plane, close to the nitrogen atom (2.591 Å) and to one of the adjacent carbon atoms (3.322 Å). Interestingly, the two hydrogen atoms bear a considerable charge separation, the one closer to nitrogen being positively charged and the other negatively charged (see Table 1). This charge separation suggests some non-negligible electrostatic contribution to the BE, possibly reflected in the notably larger PW91 computed BE, compared to the MP2 result (1.00 kcal/mol for the same structure). The top site (Figure 3b) is predicted to be less stable than the edge site at the DFT level, but the stability difference is practically removed at the MP2 level (BE of 0.95 kcal/mol). The BE of the top site is smaller than that of benzene, but the interesting result is that pyridine possesses at least two different sites for H_2 physisorption characterized by approximately the same stability, which might lead to a larger number of H_2 molecules stored in the vicinity of a pyridine-containing material.

DFT calculations predict two slightly different H_2 complexes with the n-oxide derivative of pyridine (see Figure 4a,b and Table1). In both complexes the molecular hydrogen sits on the top of the molecular plane, but in one case (Figure 4a) the H_2 molecule is close to the oxygen (2.426 Å), to the nitrogen (2.986 Å) and to one of the adjacent carbon atoms of the aromatic ring (3.351 Å), whilst in the second case (see Figure 4b) the H_2 molecule, always on top of the molecular plane, is symmetrically located along the axis of the NO bond, and it is close mainly to the oxygen atom (2.481 Å). The two sites are characterized by similar stabilities (1.23 and 1.17 kcal/mol), and in both cases the NBO atomic charge separation on the two hydrogen atoms of H_2 is considerable (see Table1). The two optimized structures represent two shallow minima on a very flat potential energy surface in the vicinity of the NO bond. Indeed, a more realistic interpretation of this result is that, according to the PW91/6-311++G** results, the H_2 molecule can move almost freely from one structure to the other. The MP2/aug-cc-pVTZ optimizations starting from the above two structures converged to a single complex, similar to the DFT result of Figure 4b, although in this case the H_2 molecule is oriented toward the NO bond and it is much closer to the nitrogen atom (2.640 Å), compared to the DFT result (3.291 Å). Shortly, at the MP2 level the potential energy surface presents a minimum for a structure that is somewhat intermediate between the two DFT shallow minima. The computed BE (1.40 kcal/mol) is also not too far from the less expensive

DFT result, and its considerable value casts n-oxide pyridine among the more interesting alternatives to benzene for carbon based materials with better hydrogen storage performances.

FIGURE 5 HERE

FIGURE 6 HERE

FIGURE 7 HERE

Five-atom-rings. To extend the range of possible alternatives to benzene in carbon based materials, we have considered the H_2 interaction with furan, pyrrole and tiophene. In all three cases we have found two possible H_2 sites: the usual top site and an edge site in which the H_2 molecule is located in the - or across the - molecular plane, and close to the hetero-atom. The computed PW91/6-311++G** structures are depicted in Figures 5, 6 and 7.

The two sites found for furan have similar BE, namely 0.64 kcal/mol for the edge site shown in Figure 5a and 0.70 kcal/mol for the top site shown in Figure 5b. In the edge site the H_2 molecule sits on the molecular plane, and is oriented along the symmetry plane perpendicular to the molecular plane. The computed BE of the two sites are similar to those of benzene itself, a result suggesting that materials based on furan would not perform better than benzene itself. It is perhaps of some interest, however, that each furan, similarly to pyridine, possesses two different H_2 sites of similar stability. A similar, although more interesting situation occurs for pyrrole, for which the PW91/6-311++G** calculations predict an edge site with a BE of 0.75 kcal/mol (see Figure 6a and Table 1) and a top site with a larger BE of 1.03 kcal/mol. In the edge site the molecular hydrogen is close to the NH bond and located along NH line, but it crosses the molecular plane so that one H atom is above the plane and the other is below. Given the large BE of the top site structure, we have supplemented the DFT calculations with MP2/aug-cc-pVTZ geometry optimization and found two structures similar to those predicted from DFT calculations, as indicated by the red geometrical parameters shown in Figures 6a,b. Interestingly, the MP2 predicted BE of the edge site is very close (0.61 kcal/mol) to the DFT result and, as in the case of the edge structure of pyridine, it is predicted to be slightly lower than the DFT result. Conversely, the MP2 predicted BE of the top site follows the generally observed trend by providing a larger value (1.33 kcal/mol) than the DFT result, and it confirms the larger stability of the top site of pyrrole compared to benzene. Thus, pyrrole can also be considered an interesting compound to induce larger binding of molecular hydrogen in carbon based materials. The last five-ring hetero-aromatic compound considered, tiophene, also forms two different H_2-complexes, but the edge site (see Figure 7a), analogous to the edge site of furan, is much less stable since its BE is only 0.35

kcal/mol. The computed BE for the top site, on the other hand, is 0.75 kcal/mol that is, almost the same as that of benzene. Thus, based on these predictions we can conclude that materials replacing benzene rings with tiophene or derivatives should not show improved H_2 storage capacities. The above results might explain why replacement of the phenylene moiety with tieno[3,2-b]tiophene in MOF materials did not produce significant improvements in the H_2 storage performance at low pressure [30] while the good performance detected at higher pressures [15] can be explained in terms of a favorable combination of surface area and density [15] rather than in terms of stronger interactions with the organic linker.

Larger aromatics

The stability of molecular hydrogen adsorption sites was investigated also for larger polar and hetero-aromatic molecules. From the previous discussion it emerges that the more stable H_2 sites are found for pyrrole, pyridine and n-oxide pyridine. Although the top site of pyrrole shows the largest BE, the edge site of pyridine is particularly interesting since short oligomers of pyridine may form bidentate or terdentate ligands for molecular hydrogen and are expected thereby to increase the strength of the binding. For this reason we first explored the H_2 binding properties of bipyridine and tripiridine. The resulting complexes are depicted in Figures 8a and 9.

FIGURE 8 HERE

FIGURE 9 HERE

To evaluate the effect of the bidentate ligand, we restricted the attention to the *cis* isomer of bipyridine and considered the complex of the edge type in which molecular hydrogen can interact with both nitrogen atoms. The computed PW91/6-311++G** equilibrium structure is shown in Figure 8a. The two rings of bipyridine are computed to be twisted by 35º and the H_2 molecule is located closer to one of the two nitrogen atoms to maximize the interaction with one pyridinic ring. The smaller N--H_2 distance (2.678 Å) is indeed very close to the distance in pyridine (2.591 Å). Since the second pyridinic nitrogen is at a larger distance, its contribution to the total BE is expected to be reduced. Indeed, the computed BE is 1.32 kcal/mol, which is only 14% larger than the BE of pyridine-H_2 at the edge site. Nevertheless, the second pyridinic ring in bypiridine contributes to create a very favourable H_2 adsorbing site with partial electrostatic character, as shown by the considerable charge separation on the H_2 molecule (see the NBO charges on Table1). This edge site sums up to the top sites located over each pyridinic ring.

With a similar objective in mind, namely the maximization of the H_2 binding through multiple local interactions with the aromatic compound, we considered also the complex formed by molecular hydrogen and the highly polar pyrene-4,5-dione that possesses two close C=O groups. It has been shown recently, that a rather strong dipole-dipole intermolecular interaction drives the formation of alternating stacked arrays of these polar molecules[31]. The computed structure of the complex with molecular hydrogen is depicted in Figure 8b: the H_2 molecule is located on the molecular plane and is slightly closer to one of the two oxygen atoms. Although the charge separation on the H_2 molecule is remarkable (see Table 1), the computed BE is only 0.97 kcal/mol.

In Figure 9 we report the structures of the complexes of H_2 with tripyridine. We considered two conformers of *cis,cis* tripyridine, namely one with a C_2 axis passing through the central pyridinic ring (Figure 9a) and one with a plane of symmetry passing through the central pyridinic ring (Figure 9b). The former corresponds to the more stable conformer for the isolated molecule, but owing to the larger distance of the two nitrogen atoms belonging to the external pyridinic rings (5.064 Å in the C_2 isomer, and 4.824 Å in the C_s isomer), it is expected to interact less efficiently with molecular hydrogen. The computed BEs confirm this hypothesis with a slightly larger interaction (1.41 kcal/mol) for the C_s isomer than for the C_2 isomer (1.35 kcal/mol). In both cases the hydrogen molecule is closer to one of the external pyridinic rings. The structure of the complex with the C_2 isomer of tripyridine resembles that with bypiridine, since the N--H_2 distances are 2.698, 3.158 and 3.994 Å, with the first two very close to those found for bypiridine and the third pyridinic ring negligibly interacting with H_2. This is confirmed by the computed BE which is 1.35 kcal/mol (1.32 kcal/mol for bypiridine). The N--H_2 distances in the complex with the C_s isomer of trypiridine are 2.690, 3.548 and 3.697 Å. Thus, one pyridinic ring forms a complex with structure similar to pyridine, while the additional two pyridinic rings provide approximately a similar contribution to the total BE of 1.41 kcal/mol, which represents an interesting value for a carbon based compound. Based on the results on pyridine, these predicted PW91/6-311++G** stabilities are expected to be comparable with the MP2/aug-cc-pVTZ predictions.

FIGURE 10 HERE

The last polar aromatic compound considered is n-phenyl-aniline. The interaction of H_2 with aniline (top site) was considered in a recent study and it was predicted to be ca 16 % larger compared to benzene [8]. Beside the top site interaction of H_2 with one of the two phenyl ring of n-phenyl-aniline, we considered several other H_2 approaches and found two

additional H_2 sites. The structures of the three complexes obtained at PW91/6-311++G** level are presented in Figure 10. The first structure (Figure 10a) corresponds to the already mentioned top site, and its binding is computed to be 0.80 kcal/mol. This value is certainly underestimated, with respect to more sophisticated MP2 results, as is the case for all the top sites considered in this work (see Table 1). Nevertheless, in keeping with the calculations reported earlier for aniline, it is larger than the BE of the top site of benzene. The second structure shown in Figure 10b, corresponds to H_2 interacting with the edge side of the molecule and it is similar to the edge site discussed for pyrrole. The computed BE is also similar (0.72 kcal/mol) to that of the edge site of pyrrole (0.75 kcal/mol). Finally, H_2 can be weakly bound (BE 0.64 kcal/mol) to n-phenyl-aniline with a structure, shown in Figure 10c, that corresponds to a top site located over the NR_2H group. Although none of the interacting sites is particularly stable, it is interesting to note that n-phenyl-aniline can interact with several hydrogen molecules through its multiple sites.

FIGURE 11 HERE

H_2 stretching frequency and infrared activity

As discussed in a previous section, vibrational frequencies (and infrared intensities) were computed for each aromatic-H_2 complex optimized at PW91/6-311++G** level of theory. It is thus of some interest to analyze the computed stretching frequencies of H_2 and their activities in the various complexes formed by the molecule with polar aromatic compounds. The stretching frequency of isolated H_2, computed at the same level of theory, is overestimated (4337 cm^{-1}) with respect to the experimental value [32] (4161 cm^{-1}). However, the computed frequency lowering upon complexation and the associated infrared intensities are expected to correlate with the perturbation induced on the H_2 molecule by the aromatic compound. To this end we have plotted, in Figure 11, the computed infrared intensities against the computed H_2 stretching frequencies. Inspection of Figure 11 shows that there is a reasonably linear correlation between the two molecular properties. In addition, if one considers also the computed binding energies, it is seen that most complexes possessing bindings above 1.00 kcal/mol fall in the top-left portion of Figure 11. The case of pyridine is however particularly interesting: the two sites available for H_2 in pyridine are predicted to show rather different spectroscopic behaviour: the edge site is predicted to be characterized by a considerably lower H_2 stretching frequency and large IR intensity, conversely, the top site is predicted to induce a minor frequency lowering and negligible infrared intensity. This different behaviour is possibly related to the increased electrostatic contribution in the BE of

the edge site compared to the top site and it suggests that the edge site should be easily detected in infrared studies. The same conclusion holds for the edge sites in bypiridine or trypiridine.

FIGURE 12 HERE

FIGURE 13 HERE

H_2 sites in MOF materials

We have restricted our study to the interaction of molecular hydrogen with the metal-oxide corner of MOF materials and we have adopted the same model already employed by other authors [9,19], namely the $OZn_4(CO_2H)_6$ cluster shown in Figures 12 and 13.

We have considered several approaching directions for the H_2 molecule that lead, after geometry optimization at the PW91/6-311++G** level of theory, to three optimized complexes shown in Figures 12 and 13. Interestingly, the three structures correspond to H_2 sites detected in recent experimental studies [16-19] and here we chose preferentially to follow the labelling scheme adopted in ref. [17] to identify them. The first structure, shown in Figure 12a corresponds to the cup site of ref. [17], (α-site in ref. [18]) and its computed BE is 0.64 kcal/mol. For this H_2 site we also performed a geometry optimization with the same PW91 functional and the computationally cheaper Lanl2DZ basis set [33,34] and found a BE of 0.58 kcal/mol. In the optimized structure (see Figure 12a) the distances of the H atoms from the central oxygen atom are 4.051 Å and 4.072 Å respectively but the gas molecule is much closer to the zinc and oxygen atoms forming the cup. This structure is similar to that determined in previous computational studies in which the binding energy was computed to be 1.64 kcal/mol [9] or 0.54 kcal/mol [19]. In particular, the orientation of the H_2 molecule (inside the cup site) found by us is closer to the η^2-O structure reported in ref. [19]. Our computed value is in between these previous calculations and interestingly, it is closer to the recently estimate of ca. 0.84 kcal/mol obtained from temperature dependent infrared studies [19]. The second structure shown in Figure 12b corresponds to the ZnO_3 site of ref. [17] or the β-site of ref. [18]. We computed a lower BE for this site, namely 0.49 kcal/mol, in agreement with the observation of lower stability for this site [17]. This structure corresponds to the η^2-Zn structure computed in ref. [19] and the main H_2 distances from the metal-oxide are indicated in Figure 12b. Finally, we determined a third site (see Figure 13) in which the H_2 molecule is close to one of the external oxygen atoms of the metal-oxide cluster and we can associate this site to the less stable hex site detected in ref. [17]. In contrast with the

experiment, the BE of this site is computed to be larger than that of the cup site, but the larger computed stability (0.76 kcal/mol) results from the truncated model considered here. Indeed, the stability of H_2 in this site would be greatly reduced if the organic linker had been included in the model, since in the complete MOF structure, the H_2 molecule would be strongly destabilized by the repulsion with atoms belonging to the organic linker.

In summary, the computed results indicate a larger stability for the cup site, in agreement with experimental observations and with recent calculations at MP2 level [19]. The computed BE energies are also very close to the experimental determinations [19].

Concluding remarks

To improve the hydrogen storage efficiency of carbon based materials it is crucial to increase the stabilization of hydrogen molecules on the surface. This can be obtained by increasing the electrostatic contribution to the surface-H_2 physical interaction, which is usually dominated by dispersion forces. One way to do that is through chemical modification of the carbon based material, namely by introducing polar groups or hetero-atoms.

We have investigated, with quantum-chemical calculations on model systems, whether chemical substitution on carbon based materials, may be considered a valid strategy to increase the strength of the physisorption, to obtain more promising materials for hydrogen storage. To this end we have considered several hetero-aromatic compounds or substituted benzenes and investigated the BSSE corrected binding energies of molecular hydrogen sites with DFT calculations employing the PW91 exchange-correlation functional and the 6311++G** basis set, supplemented by MP2/aug-cc-pVTZ validations for selected H_2-complexes. While the DFT binding energies are generally underestimated for pure dispersive interactions, they become closer to the MP2 values for increasing electrostatic contributions. Furthermore, the PW91 computed binding energies for the H_2 sites close to the metals-oxide corner of MOF materials are in good agreement with experimental observations.

Among the compounds investigated, a moderate increase of the binding energy has been computed for pyrrole, pyridine, oligomers of pyridine, and n-oxide pyridine. At the same time, for some hetero-aromatic molecules it has been shown that edge sites, beside the top sites, become competitive for H_2 physisorption. Nevertheless, based on the computed binding energies we can conclude that carbon based materials including the most performing polar aromatics considerd in this work would not show the required storage capacities for practical applications. Nonetheless, the ideas developed here may be used to design new storage media. For instance, replacement of the phenylene moiety with pyridine or bypiridine in MOF

materials may prove to enhance the adsorption on edge sites recently indicated as important sites for the organic linkers of these mixed organic-inorganic materials [14,16].

Finally, calculations have also indicated a correlation between the infrared activity of the H_2 stretching mode and its frequency in the complex and a different spectroscopic behaviour for different H_2 sites of the same compound. In particular, the edge and top sites of pyridine are expected to be easily distinguished by their remarkable different spectroscopic parameters.

Acknowledgements

This work was supported by funds from MURST PRIN 2004 (project: "Spettroscopia rotazionale in assorbimento e a trasformate di Fourier: Produzione e studio di nuovi cluster e specie molecolari in espansioni supersoniche"), MURST ex 60% (Project: "Modelli per lo studio delle proprietà di sistemi molecolari complessi") FIRB 2001 (project n. RBNE019NKS). We are indebted with Prof. Klaus Müllen for helpful discussions and with the referees for useful comments and suggestions.

References

1. Schlapbach L, Zuttel A, (2001) Nature 414:353-358.
2. Schimmel HG, Kearley GJ, Nijkamp MG, Visserl CT, de Jong KP, Mulder FM, (2003) Chem Eur J 9:4764-4770.
3. Vidali G, Ihm G, Kim HY, Cole MW, (1991) Surf Sci Rep 12:133-181.
4. Mattera L, Rosatelli F, Salvo C, Tommasini F, Valbusa U, Vidali G, (1980) Surf Sci 93:515-525.
5. Hirscher M, Becher M, Haluska M, von Zeppelin F, Chen XH, Dettlaff-Weglikowska U, Roth S, (2003) J Alloys Compd 356:433-437.
6. Tran F, Weber J, Wesolowski TA, Cheikh F, Ellinger Y, Pauzat F, (2002) J Phys Chem B 106:8689-8696.
7. Heine T, Zhechkov L, Seifert G, (2004) Phys Chem Chem Phys 6:980-984.
8. Hubner O, Gloss A, Fichtner M, Klopper W, (2004) J Phys Chem A 108:3019-3023.
9. Sagara T, Klassen J, Ganz E, (2004) J Chem Phys 121:12543-12547.
10. Sagara T, Klassen J, Ortony J, Ganz E, (2005) J Chem Phys 123:014701.
11. Buda C, Dunietz BD, (2006) J Phys Chem B 110:10479-10484.
12. Sagara T, Ortony J, Ganz E, (2005) J Chem Phys 123:214707.
13. Rosi NL, Eckert J, Eddaoudi M, Vodak DT, Kim J, O'Keeffe M, Yaghi OM, (2003) Science 300:1127-1129.
14. Rowsell JLC, Yaghi OM, (2005) Angew Chem, Int Ed Engl 44:4670-4679.
15. Wong-Foy AG, Matzger AJ, Yaghi OM, (2006) J Am Chem Soc 128:3494-3495.
16. Rowsell JLC, Eckert J, Yaghi OM, (2005) J Am Chem Soc 127:14904-14910.
17. Yildirim T, Hartman MR, (2005) Phys Rev Lett 95:art. n. 215504.
18. Spencer EC, Howard JAK, McIntyre GJ, Rowsell JLC, Yaghi OM, (2006) Chem Comm278-280.

19. Bordiga S, Vitillo JG, Ricchiardi G, Regli L, Cocina D, Zecchina A, Arstad B, Bjorgen M, Hafizovic J, Lillerud KP, (2005) J Phys Chem B 109:18237-18242.
20. Perdew JP, Wang Y, (1992) Phys Rev B 45:13244-13249.
21. Tsuzuki S, Luthi HP, (2001) J Chem Phys 114:3949-3957.
22. Dunning THJ, (1989) J Chem Phys 90:1007-1023.
23. Carpenter JE, Weinhold F, (1988) Theochem-J Mol Struct 169:41-62.
24. Boys SF, Bernardi F, (1970) Mol Phys 19:553.
25. Gaussian 03, Revision B.1, M. J. Frisch, G. W. Trucks, H. B. Schlegel, G. E. Scuseria, M. A. Robb, J. R. Cheeseman, J. A. Montgomery, Jr., T. Vreven, K. N. Kudin, J. C. Burant, J. M. Millam, S. S. Iyengar, J. Tomasi, V. Barone, B. Mennucci, M. Cossi, G. Scalmani, N. Rega, G. A. Petersson, H. Nakatsuji, M. Hada, M. Ehara, K. Toyota, R. Fukuda, J. Hasegawa, M. Ishida, T. Nakajima, Y. Honda, O. Kitao, H. Nakai, M. Klene, X. Li, J. E. Knox, H. P. Hratchian, J. B. Cross, C. Adamo, J. Jaramillo, R. Gomperts, R. E. Stratmann, O. Yazyev, A. J. Austin, R. Cammi, C. Pomelli, J. W. Ochterski, P. Y. Ayala, K. Morokuma, G. A. Voth, P. Salvador, J. J. Dannenberg, V. G. Zakrzewski, S. Dapprich, A. D. Daniels, M. C. Strain, O. Farkas, D. K. Malick, A. D. Rabuck, K. Raghavachari, J. B. Foresman, J. V. Ortiz, Q. Cui, A. G. Baboul, S. Clifford, J. Cioslowski, B. B. Stefanov, G. Liu, A. Liashenko, P. Piskorz, I. Komaromi, R. L. Martin, D. J. Fox, T. Keith, M. A. Al-Laham, C. Y. Peng, A. Nanayakkara, M. Challacombe, P. M. W. Gill, B. Johnson, W. Chen, M. W. Wong, C. Gonzalez, and J. A. Pople, Gaussian, Inc., Pittsburgh PA, 2003.
26. Weigend F, Furche F, Ahlrichs R, (2003) J Chem Phys 119:12753-12762.
27. Tang CC, Bando Y, Ding XX, Qi SR, Golberg D, (2002) J Am Chem Soc 124:14550-14551.
28. Zhou Z, Zhao JJ, Chen ZF, Gao XP, Yan TY, Wen B, Schleyer PV, (2006) J Phys Chem B 110:13363-13369.
29. Sun Q, Wang Q, Jena P, (2005) Nano Letters 5:1273-1277.
30. Rowsell JLC, Yaghi OM, (2006) J Am Chem Soc 128:1304-1315.
31. Wang ZH, Enkelmann V, Negri F, Mullen K, (2004) Angew Chem, Int Ed Engl 43:1972-1975.
32. Zecchina A, Arean CO, Palomino GT, Geobaldo F, Lamberti C, Spoto G, Bordiga S, (1999) Phys Chem Chem Phys 1:1649-1657.
33. Hay PJ, Wadt WR, (1985) J Chem Phys 82:270-283.
34. Wadt WR, Hay PJ, (1985) J Chem Phys 82:284-298.

Figure Legend

Figure 1. Front and side views of adsorption complexes between H_2 and benzene (top), benzene anion (middle), benzene cation (bottom). The more relevant structural parameters (Å) and BSSE corrected binding energies (Kcal/mol) are indicated in black (PW91/6-311++G** calculations) and in red (MP2/aug-cc-pVTZ calculations).

Figure 2. Front and side views of adsorption complexes between H_2 and benzene-BN (top), borazine (bottom). The more relevant structural parameters (Å) and BSSE corrected binding energies (Kcal/mol) are indicated in black (PW91/6-311++G** calculations) and in red (MP2/aug-cc-pVTZ calculations).

Figure 3. Front and side views of the two computed adsorption complexes between H_2 and pyridine. The more relevant structural parameters (Å) and BSSE corrected binding energies (Kcal/mol) are indicated in black (PW91/6-311++G** calculations) and in red (MP2/aug-cc-pVTZ calculations).

Figure 4. Front and side views of the two computed adsorption complexes between H_2 and n-oxide pyridine. The more relevant structural parameters (Å) and BSSE corrected binding energies (Kcal/mol) are indicated in black (PW91/6-311++G** calculations) and in red (MP2/aug-cc-pVTZ calculations).

Figure 5. Front and side views of the two computed adsorption complexes between H_2 and furan. The more relevant structural parameters (Å) and BSSE corrected binding energies (Kcal/mol) are indicated (PW91/6-311++G** calculations).

Figure 6. Front and side views of the two computed adsorption complexes between H_2 and pyrrole. The more relevant structural parameters (Å) and BSSE corrected binding energies (Kcal/mol) are indicated in black (PW91/6-311++G** calculations) and in red (MP2/aug-cc-pVTZ calculations).

Figure 7. Front and side views of the two computed adsorption complexes between H_2 and tiophene. The more relevant structural parameters (Å) and BSSE corrected binding energies (Kcal/mol) are indicated (PW91/6-311++G** calculations).

Figure 8. Front and side views of adsorption complexes between H_2 and bipyridine (top), pyrene-4,5-dione (bottom). The more relevant structural parameters (Å) and BSSE corrected binding energies (Kcal/mol) are indicated (PW91/6-311++G** calculations).

Figure 9. Front and side views of the two computed adsorption complexes between H_2 and tripyridine. The more relevant structural parameters (Å) and BSSE corrected binding energies (Kcal/mol) are indicated (PW91/6-311++G** calculations).

Figure 10. Front and side views of the three computed adsorption complexes between H_2 and n-phenyl-aniline. The more relevant structural parameters (Å) and BSSE corrected binding energies (Kcal/mol) are indicated (PW91/6-311++G** calculations).

Figure 13. Correlation between the PW91/6-311++G** computed stretching frequency of H_2 in the complexes (charged complexes are not included) and its infrared activity (in red). The reference point corresponding to the computed frequency of isolated H_2 is the green square.

Figure 12. Front and side views of two computed adsorption complexes between H_2 and a model for MOF5: the cup site (top), the ZnO_3 site (bottom). The more relevant structural parameters (Å) and BSSE corrected binding energies (Kcal/mol) are indicated (PW91/6-311++G** calculations).

Figure 13. Front and side views of an additional computed adsorption complex between H_2 and a model for MOF5: the hex site. The more relevant structural parameters (Å) and BSSE corrected binding energies (Kcal/mol) are indicated (PW91/6-311++G** calculations).

Table 1. Calculated BSSE corrected binding energies of H_2 complexes in kcal mol^{-1}

	BE (kcal/mol)[a]	BE (kcal/mol)[b]	NBO charges on H_2 [c]
Benzene	0.74	**1.11**	0.01 / -0.01
Benzene anion	0.51		0.01 / -0.03
Benzene cation	**1.05**		0.01 / 0.01
Benzene-BN	0.73		0.01 / -0.01
Borazine	0.52	0.60	0.00 / 0.00
Pyridine edge	**1.16**	**1.00**	0.02 / -0.03
Pyridine top	0.54	0.95	0.00 / -0.01
n-oxide pyridine top a	**1.23**		0.02 / -0.03
n-oxide pyridine top b	**1.17**	**1.40**	0.02 / -0.03
Furan edge	0.64		0.01 / -0.01
Furan top	0.70		0.00 / -0.01
Pyrrole edge	0.75	0.61	0.00 / 0.00
Pyrrole top	**1.03**	**1.33**	0.01 / -0.01
Tiophene edge	0.35		0.00 / 0.00
Tiophene top	0.74		0.01 / -0.01
Bipyridine edge	**1.32**		0.03 / -0.04
Pyrene-4,5-dione edge	0.97		0.03 / -0.03
Tripyridine C_2	**1.35**		0.03 / -0.04
Tripyridine C_s	**1.41**		0.03 / -0.04
n-phenyl-aniline top ring	0.80		0.01 / -0.01
n-phenyl-aniline edge	0.72		0.00 / 0.00
n-phenyl-aniline top NR_2H	0.64		0.00 / 0.00
MOF5 cup site	0.64 (0.58)[d]		
MOF5 ZnO_3 site	0.49		
MOF5 hex site	0.76		

[a] BSSE corrected PW91/6-311++G** binding energy.
[b] BSSE corrected MP2/aug-cc-pVTZ binding energy, this work.
[c] only values larger than 0.01 are listed.
[d]PW91 exchange-correlation functional with Lanl2DZ basis set.

Figure 1

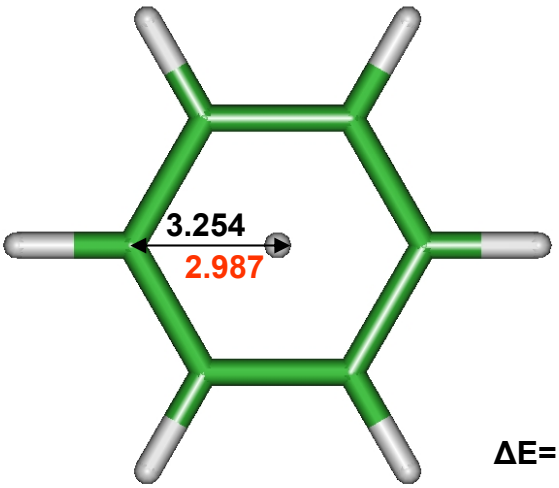

ΔE= 0.74 1.11

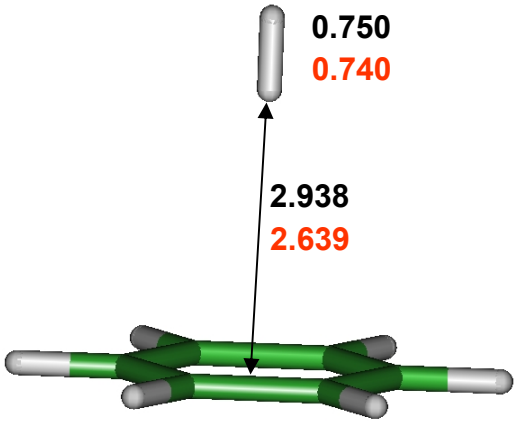

a)

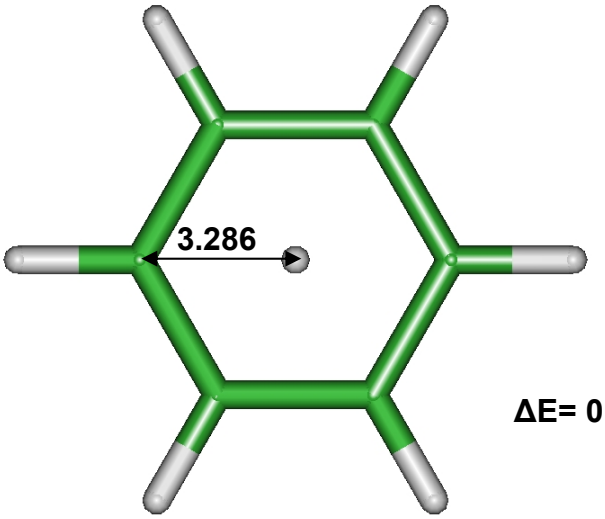

ΔE= 0.51

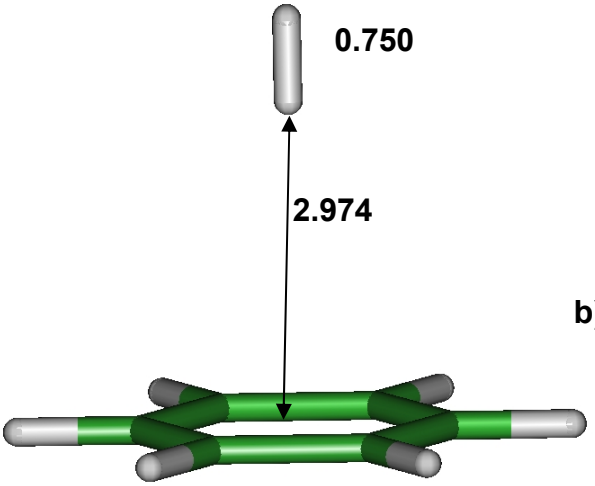

b)

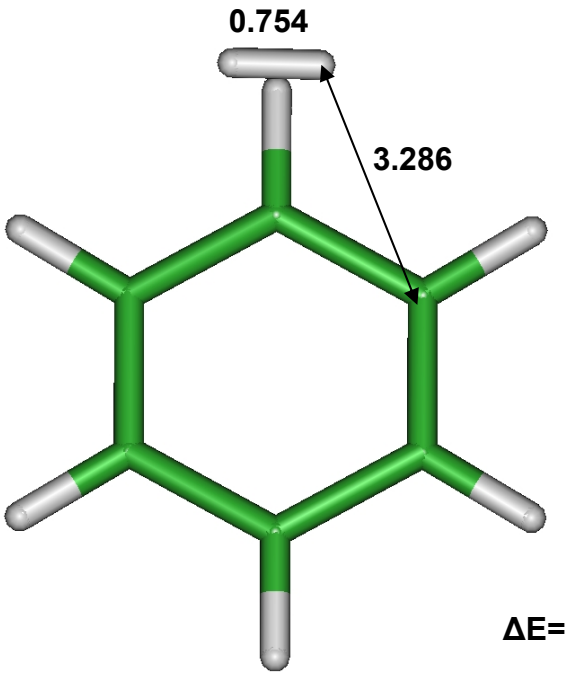

ΔE= 1.05

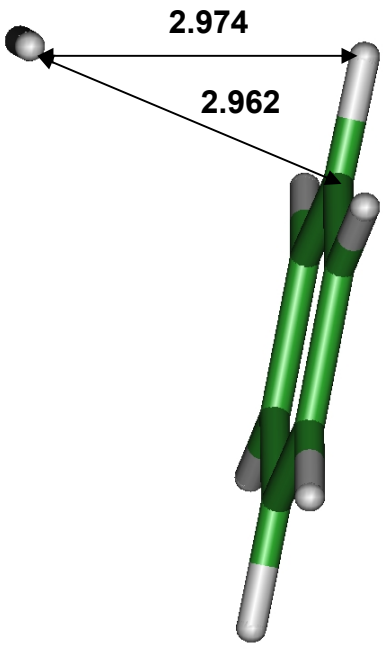

c)

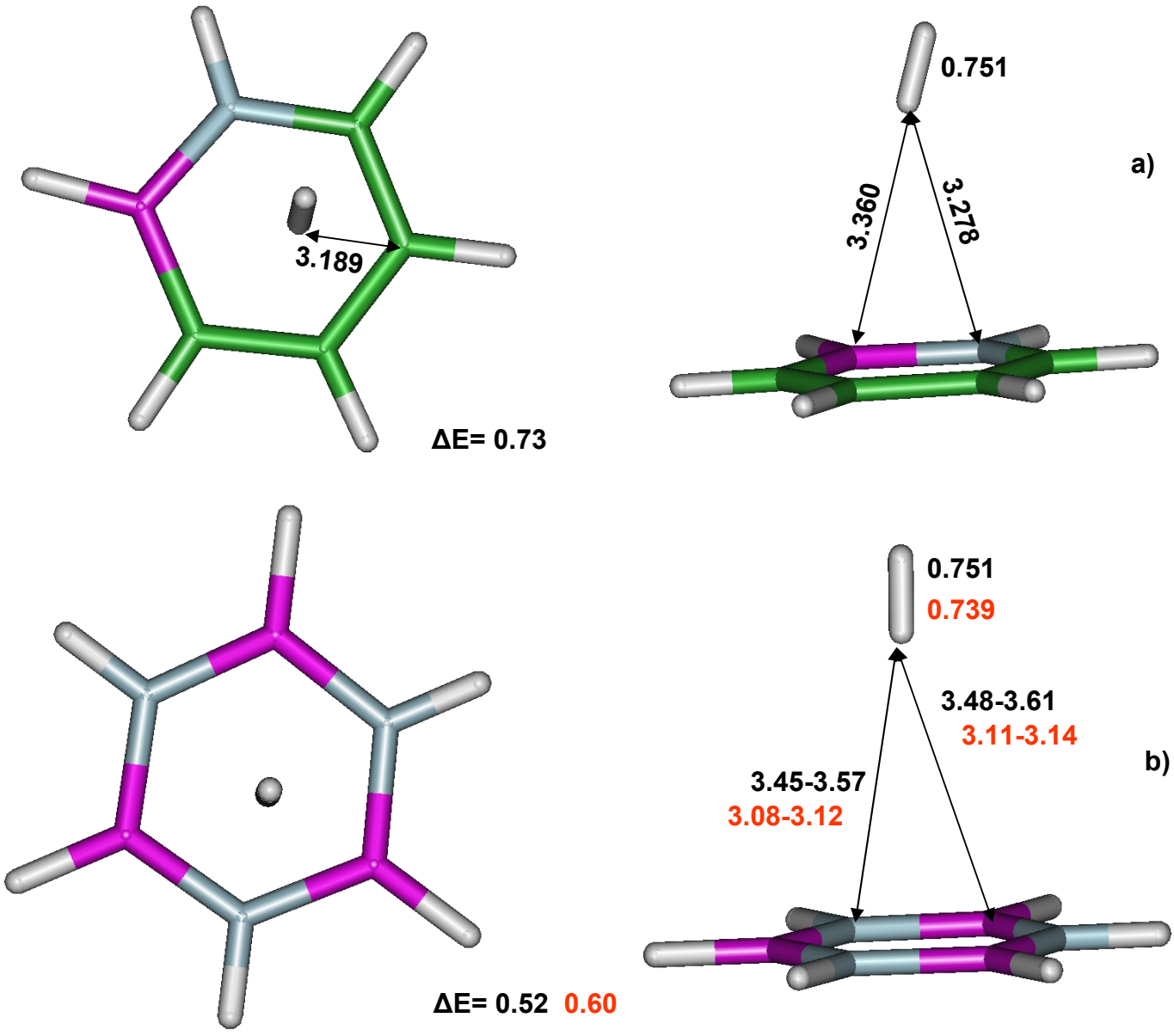
3.189
ΔE= 0.73
0.751
3.360
3.278
a)
0.751
0.739
3.48-3.61
3.11-3.14
3.45-3.57
3.08-3.12
b)
ΔE= 0.52 0.60

Figure 2

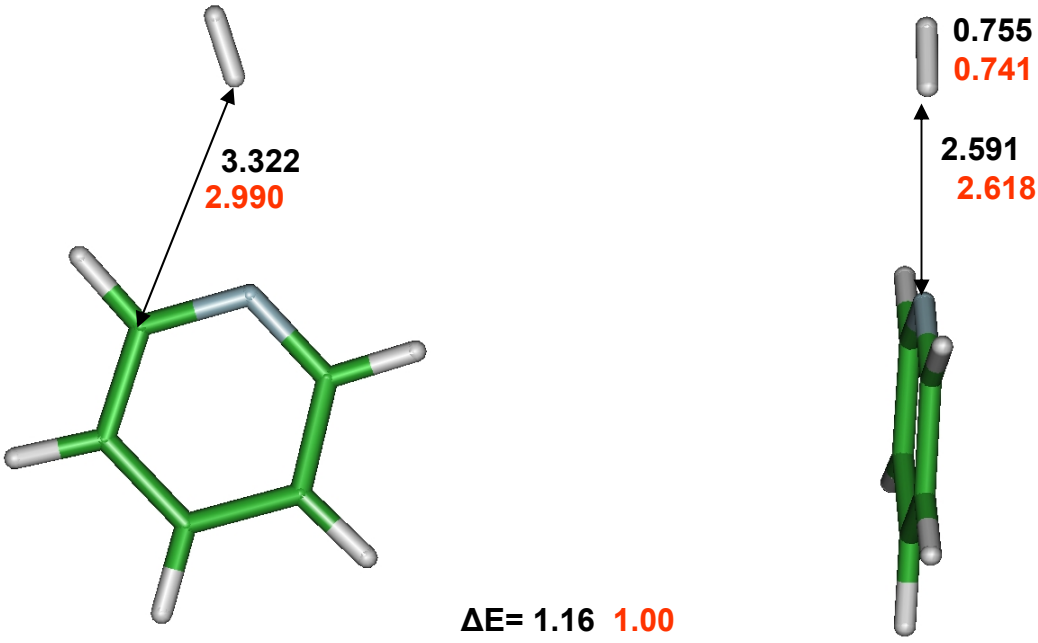
3.322
2.990
0.755
0.741
2.591
2.618
a)
ΔE= 1.16 1.00

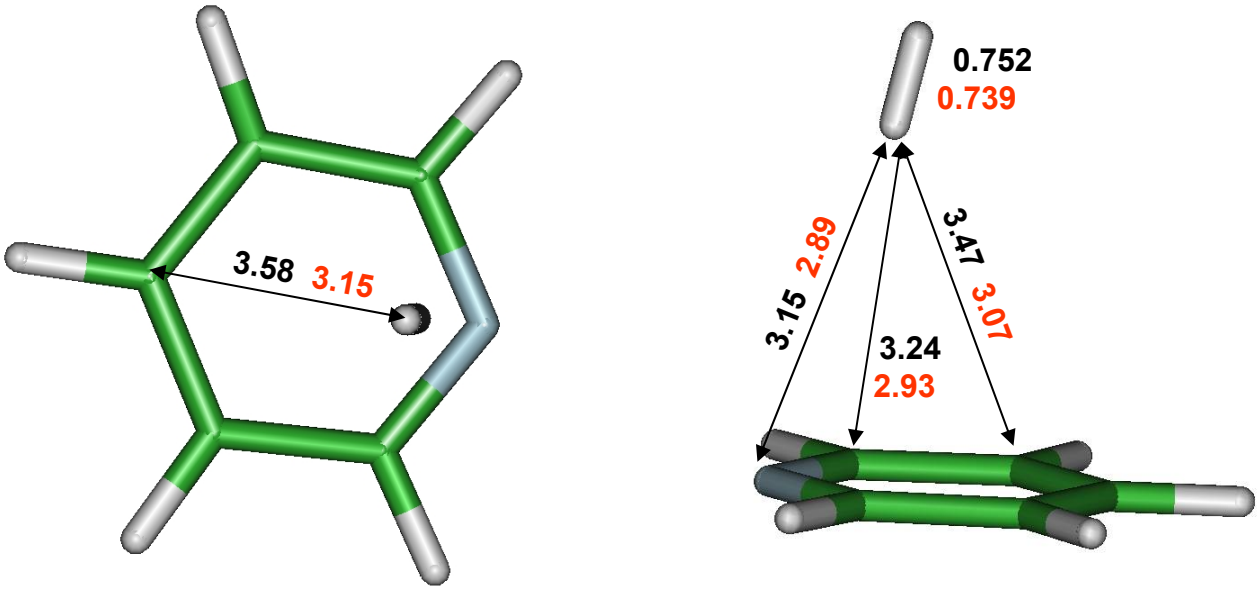
3.58 3.15
0.752
0.739
3.15 2.89
3.47 3.07
3.24
2.93
b)
ΔE= 0.54 0.95

Figure 3

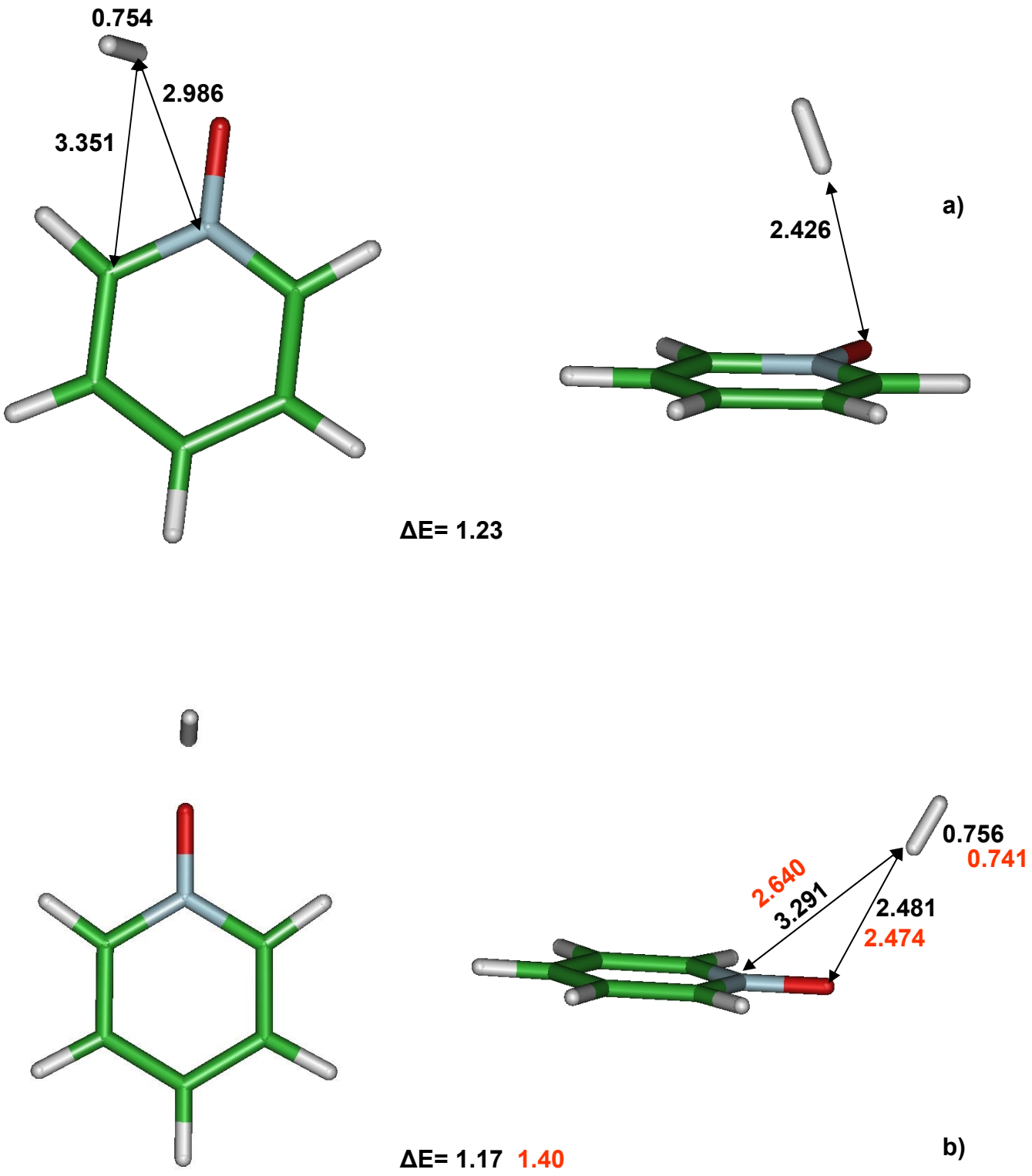
0.754
2.986
3.351
2.426
a)
ΔE= 1.23
0.756
0.741
2.640
3.291
2.481
2.474
b)
ΔE= 1.17 1.40

Figure 4

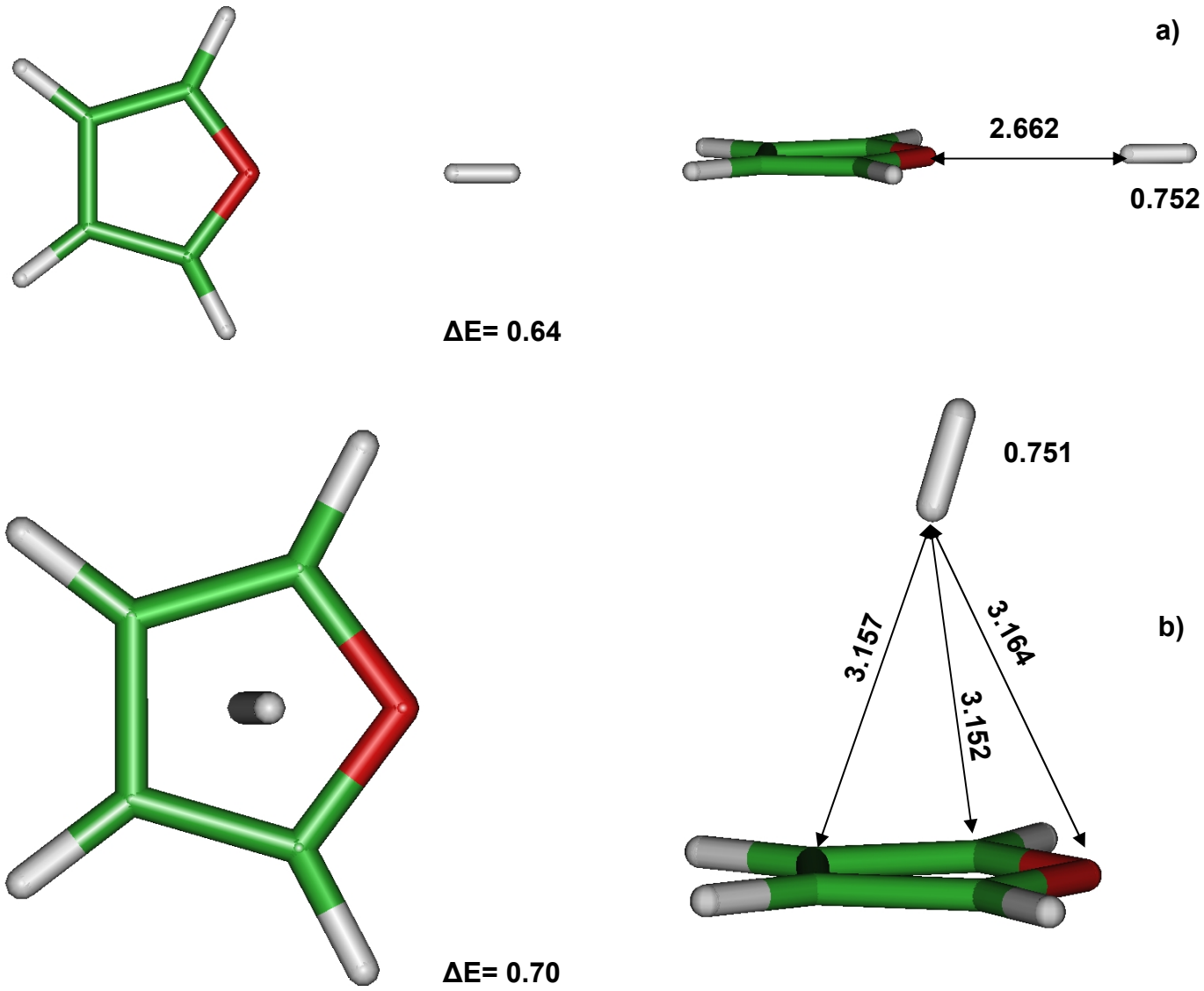

Figure 5

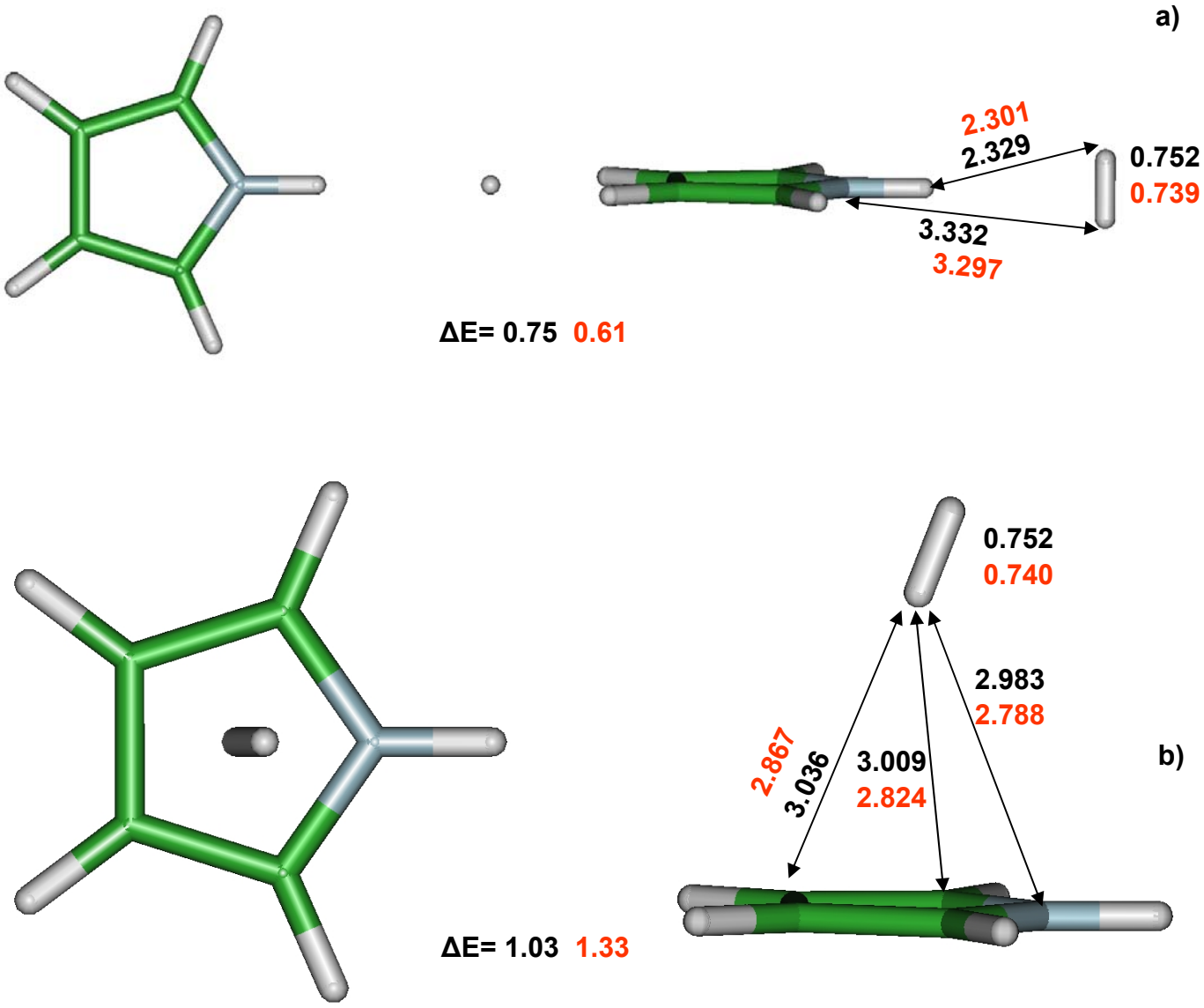
a)
2.301
2.329
0.752
0.739
3.332
3.297
ΔE= 0.75 0.61
0.752
0.740
2.983
2.788
2.867
3.036
3.009
2.824
b)
ΔE= 1.03 1.33

Figure 6

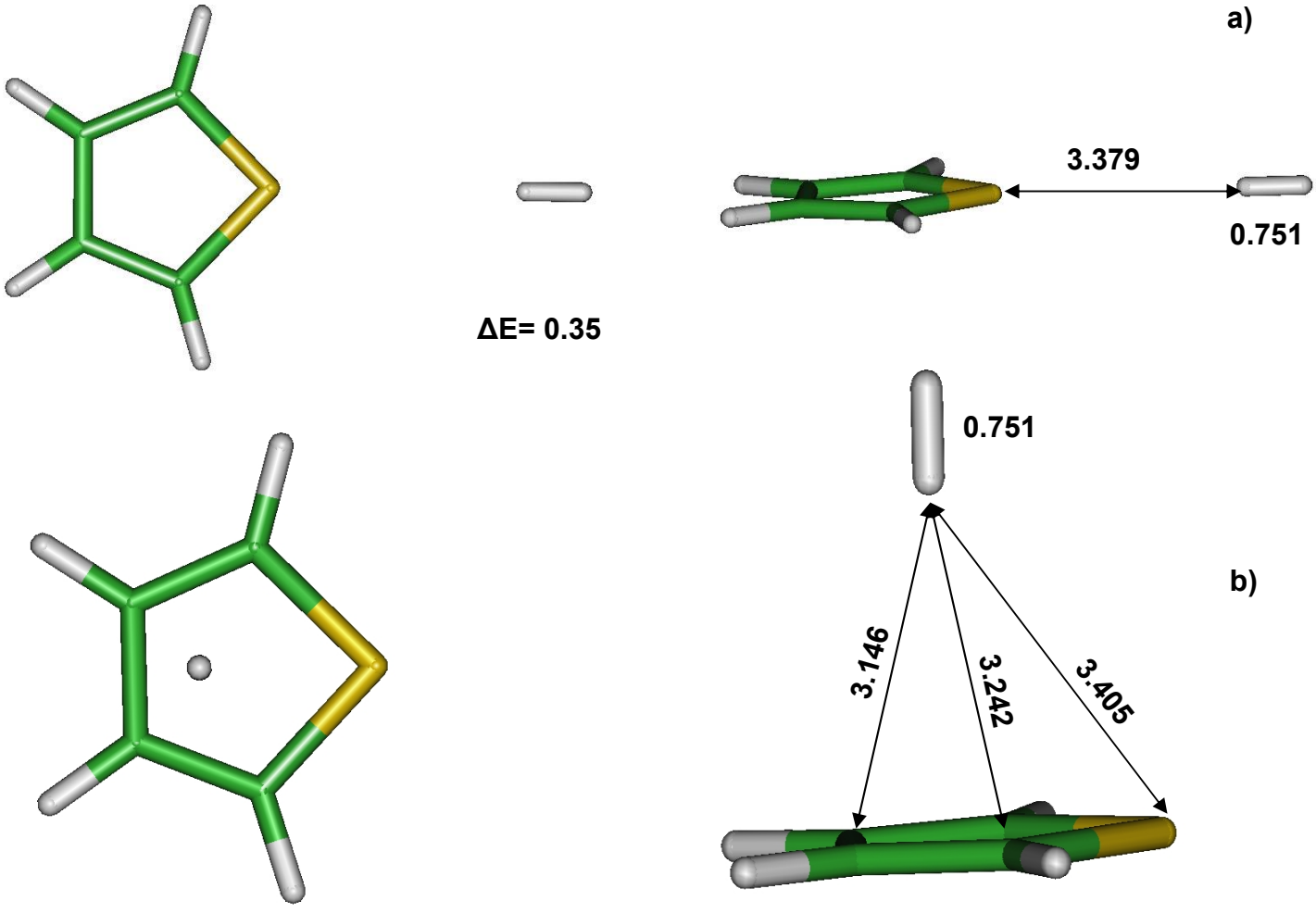

Figure 7

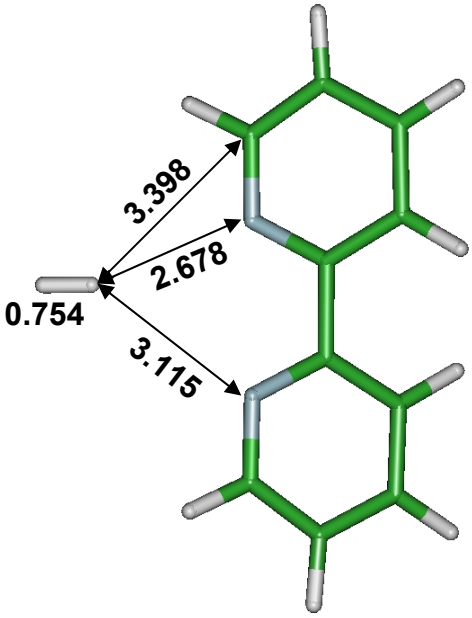

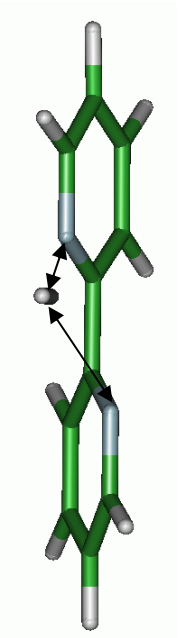

a)

ΔE= 1.32

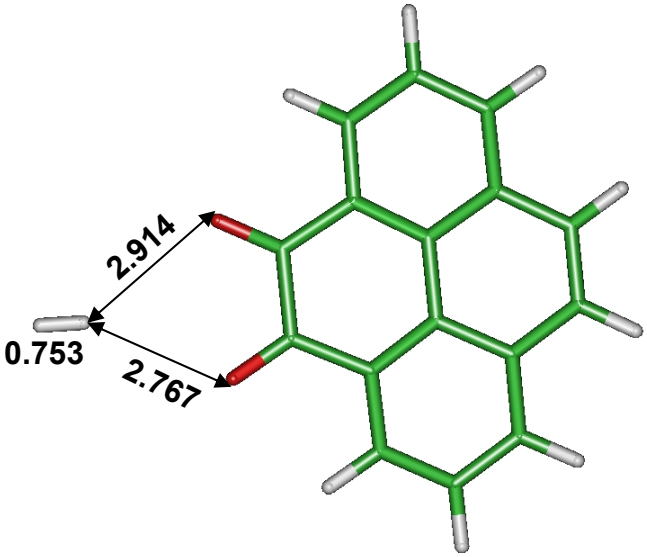

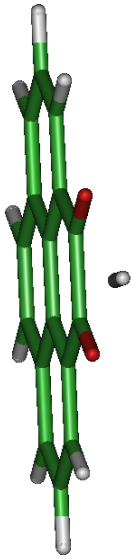

b)

ΔE= 0.97

Figure 8

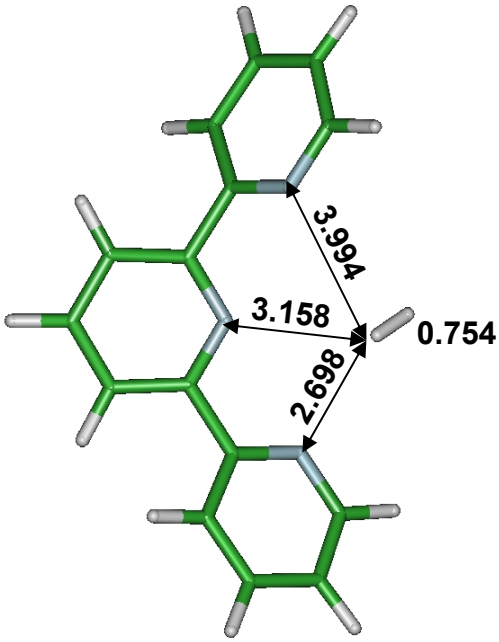

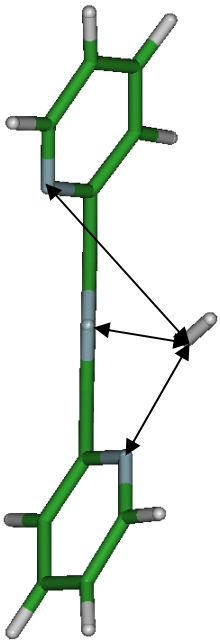

a)

ΔE= 1.35

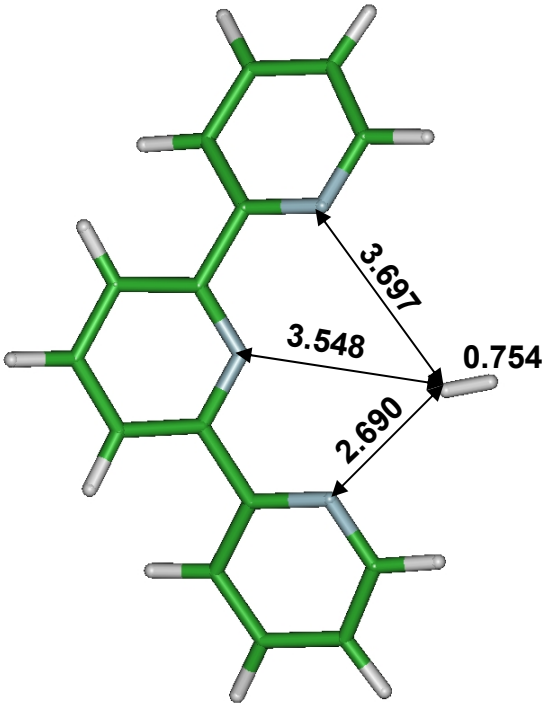

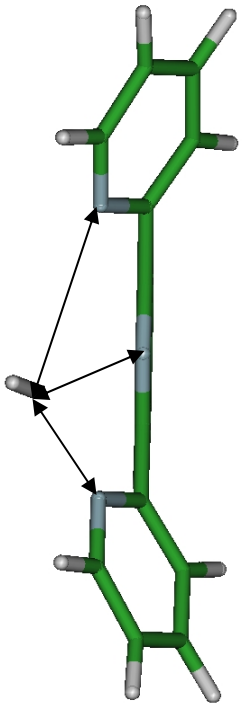

b)

ΔE= 1.41

Figure 9

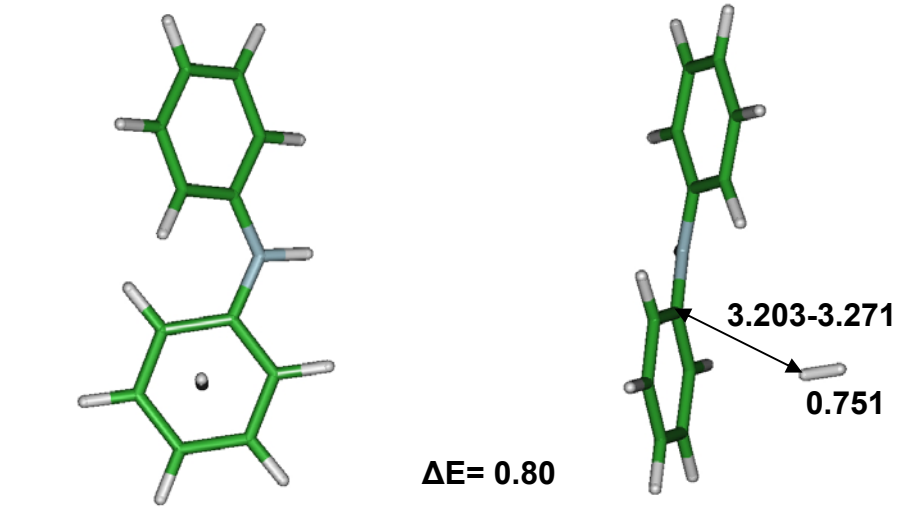

a)

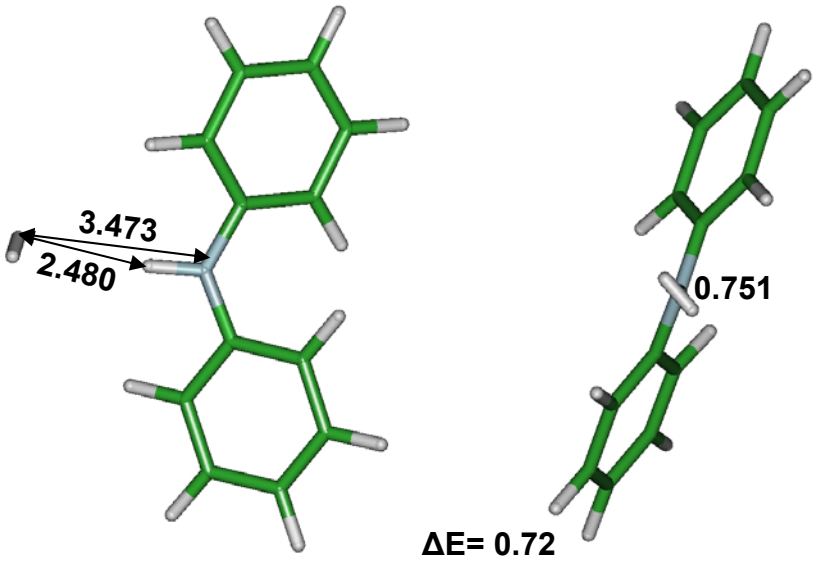

b)

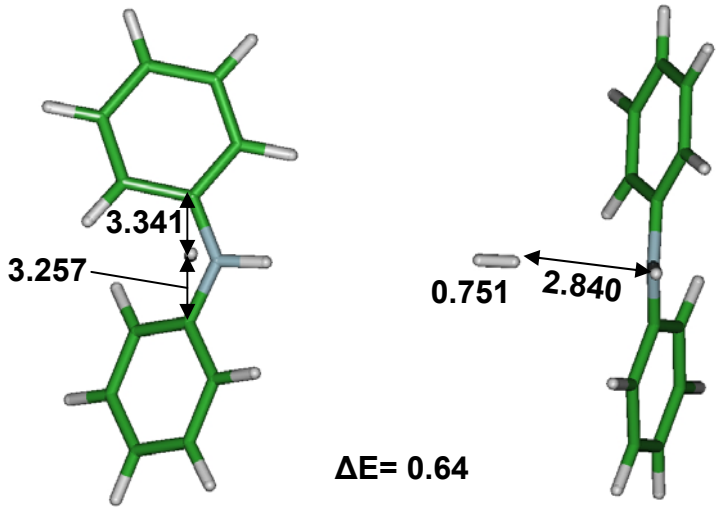

c)

Figure 10

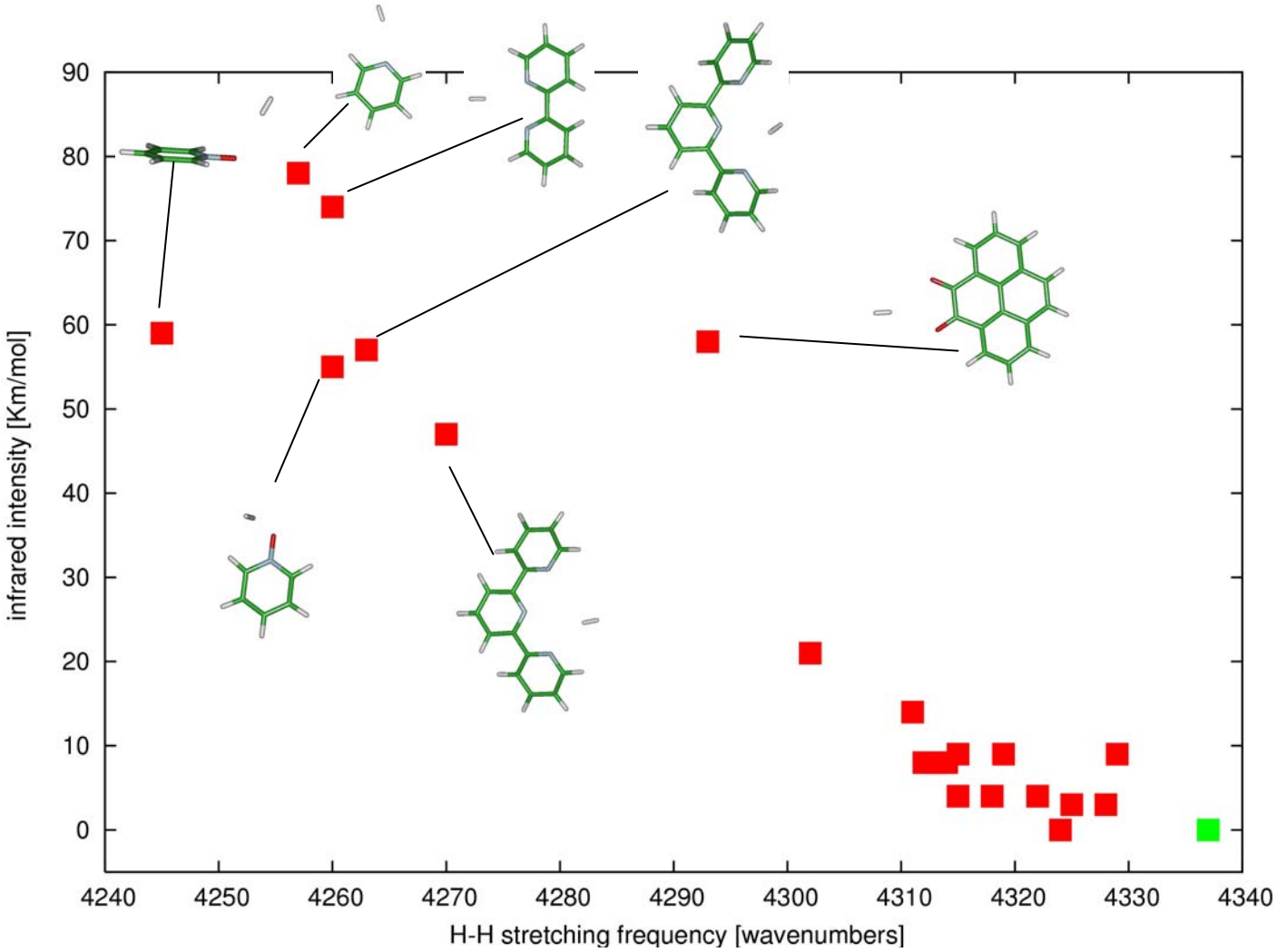
infrared intensity [Km/mol]
H-H stretching frequency [wavenumbers]
90
80
70
60
50
40
30
20
10
0
4240
4250
4260
4270
4280
4290
4300
4310
4320
4330
4340

Figure 11

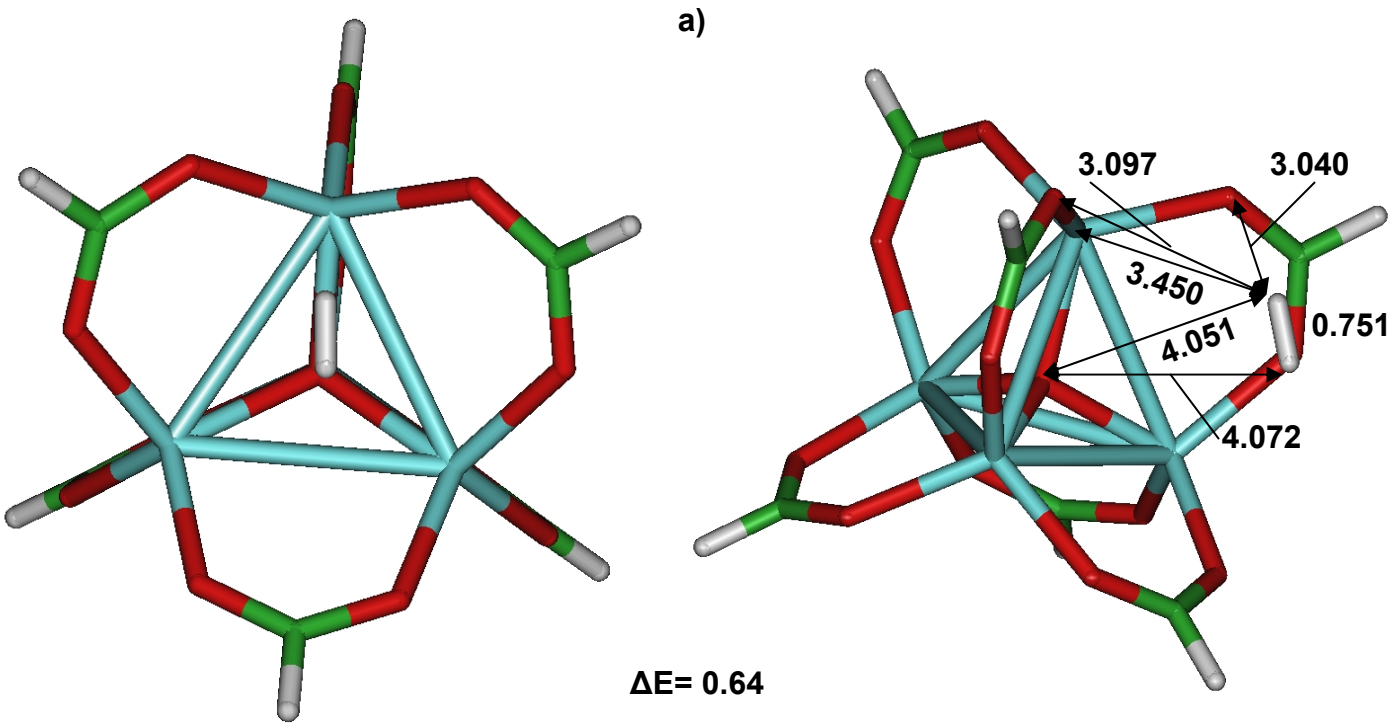
a)
3.097
3.040
3.450
0.751
4.051
4.072
ΔE= 0.64

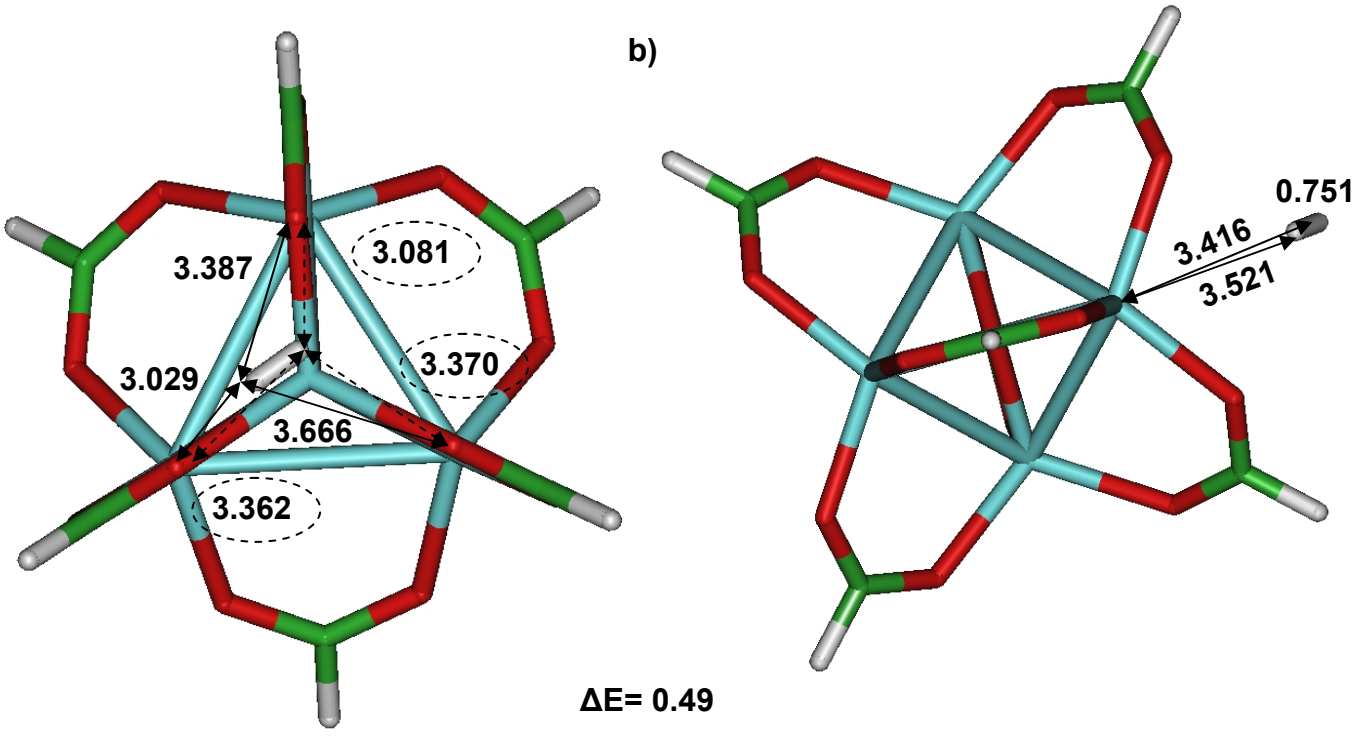
b)
3.387
3.081
3.029
3.370
3.666
3.362
0.751
3.416
3.521
ΔE= 0.49

Figure 12

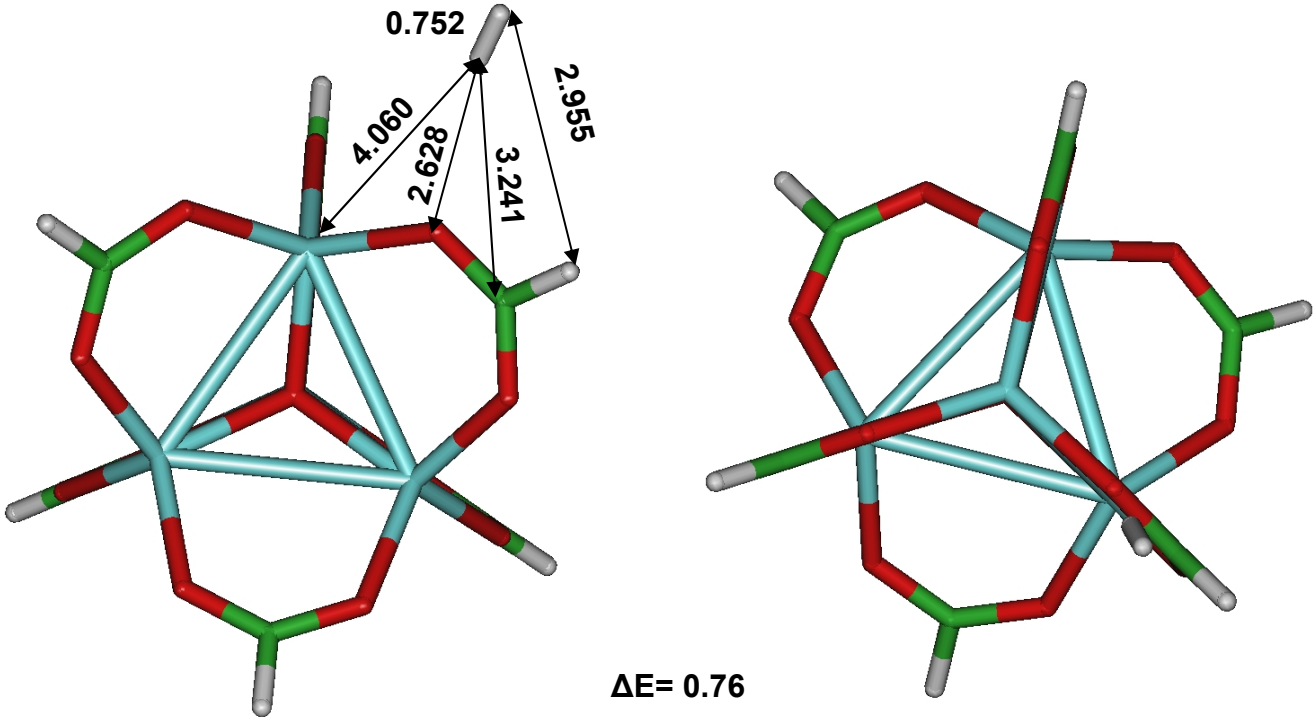

Figure 13